Formation and Structure of Self-Assembled Silica Nanoparticles in Basic Solutions of Organic and Inorganic Cations

Joseph M. Fedeyko, Dionisios G. Vlachos,* and Raul F. Lobo*

Center for Catalytic Science and Technology, Department of Chemical Engineering, University of Delaware, Newark, Delaware 19716

Received December 20, 2004. In Final Form: March 21, 2005

The phase behavior of silica solutions containing organic and inorganic cations was studied at room temperature using conductivity, pH, and small-angle scattering experiments. A critical aggregation concentration (cac) was observed at ∼1:1 ratio of SiO_2/OH^- for all cation solutions from conductivity and pH studies. From this cac, a phase diagram of the system was developed with three distinct phase regions in pseudoequilibrium: a monomer/oligomer region (I), a monomer/oligomer/nanoparticle region (II), and a gel region (III). Small-angle X-ray and neutron scattering (SAXS and SANS) on solutions of region II formed with tetrapropylammonium hydroxide (TPAOH) revealed that the nanoparticles have a core−shell structure. Structure analysis of the SAXS and SANS data was best fit by a core−shell oblate ellipsoid model. A polydisperse set of core−shell spheres also fit the data well although with lower agreement factors. Similar nanoparticle morphologies were found in solutions of TMAOH, CsOH, and NaOH.

Introduction

The development of novel silica materials with a well-defined microstructure, such as zeolites and mesoporous silicas such as MCM-41, has received much attention from the scientific community in recent years.[1,2] To this end, a quantitative understanding of the self-organization of silica would be of great help, yet important aspects of the mechanisms of silica condensation remain unknown. As an example, the role of silica nanoparticles in the formation of zeolite materials, frequently observed prior to and during growth, is still under intensive debate.[3−9] Therefore, despite progress, synthesis of new materials remains an empirical process frequently performed by trial and error.[10,11] A unifying aspect linking the formation of both microporous and mesoporous silica is the interactions between water and silica in the initial stages of the synthesis. According to Iler,[12] in aqueous solutions with a pH above 10, it is easy to form supersaturated silica solutions (compared to the solubility of amorphous silica). Here, we investigate the formation and structure of these solutions at relatively high silica concentrations.

In a previous report,[13] we showed that, in the presence of symmetric organic cations, such as tetrapropylammonium (TPA), a critical concentration of silica exists at which the homogeneous solution suddenly shifts from containing primarily monomer species to a solution containing nanoparticles as well. The formation, stability, and structure of silica nanoparticles are relevant to the homogeneous solution synthesis of silicalite-1, the siliceous form of ZSM-5, which crystallizes in the presence of the TPA cation. Many groups have shown that, in the first phase of the synthesis process, nanoparticles form within the synthesis mixture.[5−8] The importance of these particles on the mechanism for silicalite-1 growth, however, is not well-understood,[7,9,14−16] but their presence in the reaction solutions throughout the growth process suggests that they play some role in the formation of the crystalline solid.

This study focuses on answering two main questions regarding the formation of these nanoparticles. The first question is whether the formation of nanoparticles occurs solely in the presence of tetraalkylammonium (TAA) cations or whether there is a set of experimental conditions at which the nanoparticles form for many cations. We present results for sodium, cesium, tetramethylammonium (TMA), and TPA hydroxide solutions. The second issue is the determination of the shape and structure of these nanoparticles, a crucial step in understanding their stability. As previously shown,[17] temperature and initial

* To whom correspondence should be addressed. E-mail: vlachos@che.udel.edu (D.G.V.); lobo@che.udel.edu (R.F.L.). Phone: 302-831-2830 (D.G.V.); 302-831-1261 (R.F.L.).

(1) Cundy, C. S.; Cox, P. A. *Chem. Rev.* **2003**, *103*, 663.
(2) Davis, M. E. *Zeolites: A Refined Tool for Designing Catalytic Sites* (International Zeolite Symposium) **1995**, 35.
(3) Yang, S. Y.; Navrotsky, A. *Chem. Mater.* **2004**, *16*, 3682.
(4) Knight, C. T. G.; Kinrade, S. D. *J. Phys. Chem. B.* **2002**, *106*, 3329.
(5) Ravishankar, R.; Kirschhock, C. E. A.; Knops-Gerrits, P. P.; Feijen, E. J. P.; Grobet, P. J.; Vanoppen, P.; De Schryver, F. C.; Miehe, G.; Fuess, H.; Schoeman, B. J.; Jacobs, P. A.; Martens, J. A. *J. Phys. Chem. B.* **1999**, *103*, 4960.
(6) Watson, J. N.; Iton, L. E.; White, J. W. *Chem. Commun.* **1996**, *24*, 2767.
(7) Schoeman, B. J. *Microporous Mesoporous Mater.* **1998**, *22*, 9.
(8) Dokter, W. H.; Van Garderen, H. F.; Beelen, T. P. M.; Van Santen, R. A.; Bras, W. *Angew. Chem., Int. Ed. Engl.* **1995**, *34*, 73.
(9) Nikolakis, V.; Kokkoli, E.; Tirrell, M.; Tsapatsis, M.; Vlachos, D. G. *Chem. Mater.* **2000**, *12*, 845.
(10) Davis, M. E.; Zones, S. I. *Abs. Pap. Am. Chem. Soc.* **1995**, *209*, 18.
(11) Zones, S. I.; Davis, M. E. *Curr. Opin. Solid State Mater. Sci.* **1996**, *1*, 107.
(12) Iler, R. K. *The Chemistry of Silica*; John Wiley & Sons: New York, 1979.
(13) Fedeyko, J. M.; Rimer, J. D.; Lobo, R. F.; Vlachos, D. G. *J. Phys. Chem. B* **2004**, *108*, 12271.
(14) Yang, S. Y.; Navrotsky, A.; Wesolowski, D. J.; Pople, J. A. *Chem. Mater.* **2004**, *16*, 210.
(15) Kirschhock, C. E. A.; Buschmann, V.; Kremer, S.; Ravishankar, R.; Houssin, C. J. Y.; Mojet, B. L.; van Santen, R. A.; Grobet, P. J.; Jacobs, P. A.; Martens, J. A. *Angew. Chem., Int. Ed.* **2001**, *40*, 2637.
(16) Cundy, C. S.; Forrest, J. O.; Plaisted, R. J. *Microporous Mesoporous Mater.* **2003**, *66*, 143.
(17) Kragten, D. D.; Fedeyko, J. M.; Sawant, K. R.; Rimer, J. D.; Vlachos, D. G.; Lobo, R. F.; Tsapatsis, M. *J. Phys. Chem. B* **2003**, *107*, 10006.

10.1021/la0468390 CCC: $30.25
Published on Web 04/30/2005

composition can have a significant impact on particle morphology which may explain the diverging particle shape models proposed by other groups[5,8,18] for these particles. We focus on the analysis of nanoparticles synthesized at room temperature from TPA and TMA solutions.

Here, we are able to answer these questions using microstructural information gained from small-angle scattering measurements. We find that not only are these particles present in both basic organic and inorganic solutions but also the conditions of stability and particle morphology are relatively insensitive to the identity of the cations. Using a combination of pH, conductivity, small-angle X-ray scattering (SAXS), small-angle neutron scattering (SANS), and contrast matching experiments, we show that the polymerization of silica in basic solutions is a highly organized process, with a rich and complex phase behavior, and should be understood before we can rationally design functional materials. These observations are in contrast to the general view of silica polymerization as a classical polymerization process giving rise to a broad distribution of molecular structures.

Analysis of Small-Angle Scattering Data

The intensity, $I(q)$, determined in a small-angle scattering experiment is a function of multiple variables containing information about the interactions, structure, and shape of particles and is given by[19] eq 1:

$$I(q) = \Phi V^2(\rho_{\text{particle}} - \rho_{\text{solvent}})^2 P(q)\, S(q) \qquad (1)$$

Here, Φ is the particle volume fraction, ρ is the scattering length density (SLD), V is the particle volume, $P(q)$ is the particle's form factor, and $S(q)$ is the structure factor of the nanoparticle ensemble. The particle volume fraction and the difference in the scattering length density between the particle and the solvent depend on the particle and solution composition and are independent of the particle shape and other structural features. In SANS, the SLD of a particle can be determined through contrast matching experiments using mixtures of deuterated/hydrogenated solvents.[19] Information about the particle shape is included in the form factor, $P(q)$, which describes the scattering from the object, and in the particle volume, V. The effects of interparticle interactions are contained within the structure factor, $S(q)$. For dilute solutions as the ones studied here, particle interactions can be assumed to be negligible ($S(q) = 1$).[19]

For a system of monodisperse, uniform-density particles, eq 1 can be applied directly with $P(q)$ fitted using one of the various available particle shape models and $S(q)$ fitted to various interparticle force models ranging from hard spheres to charged particles in an electrolyte solution. We consider sphere, cylinder, and ellipsoid models for particle shape (i.e., $P(q)$), and the structure factor is modeled using the Hayter–Penfold mean spherical approximation. This model determines $S(q)$ for systems of charged spherical particles in a dielectric medium and can be modified to account for deviations from sphericity.[20]

To explore possible polydispersity, both $P(q)$ and $S(q)$ must be averaged over a distribution of particle sizes, according to

$$P(q) = \int F(q,r)^2\, h(r)\, \mathrm{d}r \qquad (2)$$

Gaussian and rectangular distributions of spherical particles are employed to determine the polydispersity through the weighting function, $h(r)$. The form factor, $F(q,r)$, for a spherical particle is defined as

$$F(q,r) = \frac{4\pi}{3} r^3(\rho_{\text{particle}} - \rho_{\text{solvent}}) \times \left(3\frac{\sin(qr) - qr\cos(qr)}{(qr)^3}\right) \qquad (3)$$

For spatially nonuniform particles, which have an internal distribution of SLDs, the overall form factor is determined through the addition of terms accounting for scattering from the different density regions of the particle.[21,22] The silica nanoparticles are simulated as core–shell shapes (spheres, ellipsoids, and cylinders) with a final $P(q)$ comprised of terms for the core and shell scattering.

In addition to the direct analysis of $P(q)$ and $S(q)$ from reciprocal space data, it is also possible to study small-angle scattering data in real space through the application of the pair distance distribution function (PDDF or $p(r)$), which is the inverse Fourier transform of the scattering function. The distance distribution function represents the averaged density distribution of the particle in space according to the probe radiation. $p(r)$ allows for the analysis of particle shape as well as polydispersity.[23] In addition to the shape information, the determination of $p(r)$ enables the calculation of the particle radius of gyration, R_g

$$R_g^{\,2} = \frac{\int p(r) r^2\, \mathrm{d}r}{2\int p(r)\, \mathrm{d}r} \qquad (4)$$

which for our purposes is the main metric for comparing the differences between SAXS data collected at different solution conditions.[24] R_g has the advantage of being model independent.

Materials and Methods

Silica Solution Preparation. Silica nanoparticle solutions are prepared by first diluting or dissolving the hydroxide form of the desired cation (NaOH, 98.7%, Fisher Chemicals), cesium hydroxide (CsOH, 50 wt % solution in H_2O, Aldrich), tetra-*n*-propylammonium hydroxide (TPAOH, 40 wt % solution in H_2O, Alfa Aesar), and tetramethylammonium hydroxide (TMAOH, 25 wt % solution in H_2O, Alfa Aesar) with deionized water. After stirring for 30 min in a closed Teflon vessel, tetraethyl orthosilicate (98%, Aldrich) is added to yield a final composition (molar ratio) of 9 OH^-:9500 H_2O:x SiO_2:4x EtOH. These solutions are stirred in a closed Teflon vessel for a minimum of 12 h before being analyzed. For neutron scattering studies, the nanoparticle solutions are prepared with 40% TPAOD in deuterated water. TPAOD (40 wt %) is synthesized by mixing TPABr (Aldrich) with deuterated water and silver oxide (Aldrich) in a 1.5:1 molar excess of silver oxide and stirring for 3–5 days. For the solid–liquid equilibrium studies, solutions of varying NaOH, CsOH, TPAOH, and TMAOH concentrations were prepared in the same manner with molar ratios of 4.5 or 29 OH^-:9500 H_2O. The remainder of the composition space was tested with TPAOH and TMAOH at molar ratios of 14, 18, and 40 OH^-:9500 H_2O.

(18) Watson, J. N.; Iton, L. E.; Keir, R. I.; Thomas, J. C.; Dowling, T. L.; White, J. W. *J. Phys. Chem. B.* **1997**, *101*, 10094.
(19) Feigin, L. A.; Svergun, D. I. *Structure Analysis by Small-Angle X-ray and Neutron Scattering*; Plenum Press: New York, 1987.
(20) Hansen, J. P.; Hayter, J. B. *Mol. Phys.* **1982**, *46*, 651.
(21) Arleth, L.; Pedersen, J. S. *Phys. Rev. E* **2001**, *63*, 061406.
(22) Nagao, M.; Seto, H.; Shibayama, M.; Yamada, N. L. *J. Appl. Crystallogr.* **2003**, *36*, 602.
(23) Pedersen, J. S. *J. Appl. Crystallogr.* **1993**, *1994*, 595.
(24) Glatter, O. *J. Appl. Crystallogr.* **1979**, *12*, 166.

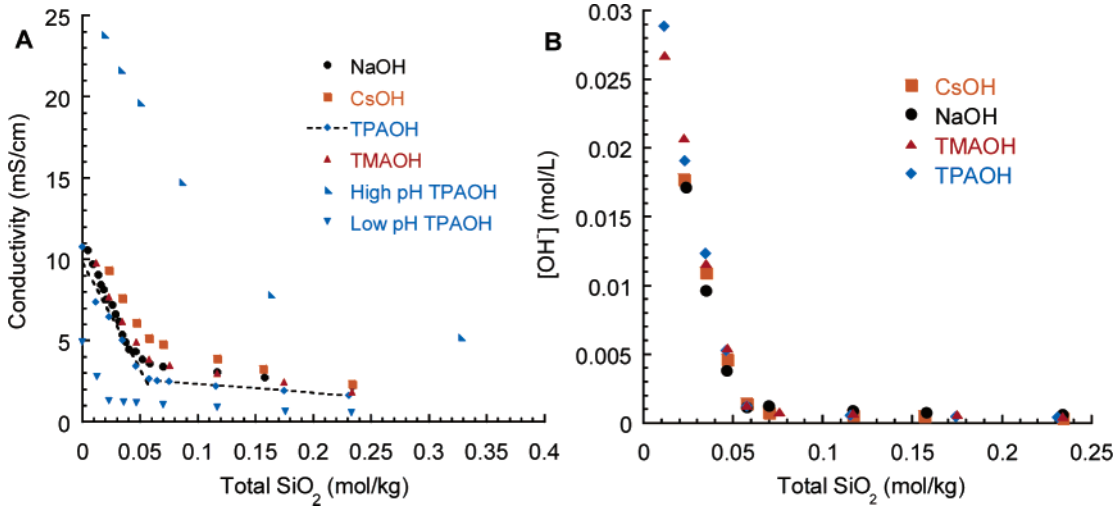

Figure 1. Determination of cac in organic and inorganic cation solutions. (A) Conductivity as a function of total silica concentration. All curves display a sudden change in slope at approximately a 1:1 SiO_2/OH^- molar ratio. After the cac, the slope is related to the ionic mobility of the cation. Variations in initial pH cause shifts of the cac to the corresponding 1:1 SiO_2/OH^- molar ratio. (B) Hydroxide concentration $[OH^-]$ as a function of total silica concentration for organic and inorganic cations. The slope change is independent of cation type and occurs at approximately the same point as that shown in the conductivity measurements.

Analytical Methods. The conductivity of the solutions is measured with a VWR model 2052 EC meter, and pH is measured using a Corning 355 pH/ion analyzer and a Corning high-performance electrode with an Ag-ion barrier. The pH meter was calibrated with standardized pH 10 and 12 buffer solutions (Alfa Aesar). The conductivity meter was tested on KCl standards at three different conductivity values (111, 12.8, 1.40 mS/cm) covering the entire conductivity range of the samples.

SANS measurements were conducted on the 30 m instrument (NG3) at the National Institute of Standards and Technology at Gaithersburg, MD. Samples were prepared following the above methods with D_2O replacing water to increase the contrast between the background and the nanoparticles. The samples were placed in quartz cells of 4 mm path length. A constant neutron wavelength of 6 Å was used with a 2.2 m sample-to-detector distance. Software provided by NIST[25] was used for the normalization of the data and the subtraction of the sample holder scattering. SAXS experiments were conducted on a SAXSess camera SAXS system (Anton-Parr). Samples were placed in a vacuum-tight 1 mm diameter quartz capillary holder and measured at 25 °C. Cu Kα radiation ($\lambda = 1.54$ Å) was used with a 265 mm sample-to-detector distance. The scattering patterns were collected on a phosphor imaging plate in the q range 0.08−8 nm^{-1}. Patterns were normalized to the height of the primary beam signal using the SAXSquant software. Desmearing was conducted by subtracting the signal from a normalized deionized water sample. Reciprocal space scattering patterns were fit using Igor Pro and a shape specific least-squares fitting algorithm (see ref 26). Both SAXS and SANS patterns were further analyzed using the generalized indirect fourier transform (GIFT) version 5-2000 software.[27] The subtracted scattering patterns were fit with a form factor followed by indirect Fourier transform to obtain pair distance distribution functions.

Contrast matching SANS experiments were conducted by varying the ratio of H_2O to D_2O in the final solution. Five contrast points are used at 25, 50, 62, 89, and 100% D_2O. At each point, the absolute intensity, $I(0)$, at $q = 0$ is determined. The square root of $I(0)$ is proportional to the scattering contrast between the particle and the solvent,[19] so if $I(0)^{1/2}$ versus $(\rho_{particle} - \rho_{solvent})$ is plotted, the point of zero contrast for the particle can be determined. This point is referred to as the scattering length density of the particle.

(25) http://www.ncnr.nist.gov/dva/index.html (data reduction web site, NIST Center for Neutron Research).
(26) Kline, S. NIST SANS fitting procedures for Igor Pro. 2001.
(27) Glatter, O.; Fritz, G.; Brunner-Popela, J.; Weyerich, B. GIFT for Windows, 1999.

Results and Discussion

Critical Aggregation Concentration in the Presence of Inorganic Cations. The conductivity and pH (Figure 1) of silica solutions has been followed in the presence of Na^+ and Cs^+ cations at compositions y [Cs^+/Na^+]:9500 H_2O:x SiO_2:4x EtOH, where $y = 4.5$, 9, and 29 and $0 < x < 145$, the same conditions used in ref 13 for symmetric organic cations. Overall, two regions are seen: at low silica concentrations, the conductivity and $[OH^-]$ drop considerably with increasing SiO_2, whereas at high silica concentrations, only slight changes occur. For an initial OH^-/H_2O ratio of 9:9500 at low concentrations of silica, the solution consists of monomers and small oligomers of silica in the protonated ($Si(OH)_4$) and deprotonated ($Si(OH)_3O^-$) forms and ions of OH^-, (Na^+/Cs^+/TPA^+, etc.), and H^+.[28] We refer to oligomeric silica as silica species not large enough to cause measurable scattering in SAXS patterns. It is known from NMR studies that under similar conditions only small oligomers are present.[29]

Although, all the charged species contribute to the conductivity of solution, OH^- is the most significant species because of its high mobility and concentration. The consumption of OH^- ions, through the deprotonation of silica with increasing fraction of silica, is therefore the cause for the drastic decrease in the solution conductivity and pH in the first region of the curves.

$$Si(OH)_4 + OH^- \leftrightarrow Si(OH)_3O^- + H_2O \qquad [R_1]$$

In the second regime, the consumption of OH^- slows down with increasing fraction of silica.

By dividing the curves into two different regions and fitting the linear portion of the curves, a critical aggregation concentration (cac) of the solution can be determined. Particles are observed by SAXS only after this cac has been crossed (see below). The cac values calculated from both conductivity and pH curves (see below) are between 0.047 and 0.058 mol/kg, which represent a variation in the [TEOS]/$[OH^-]$ ratio from 0.89:1 to 1.09:1 for Cs^+ to

(28) Kinrade, S. D.; Knight, C. T. G.; Pole, D. L.; Syvitski, R. T. *Inorg. Chem.* **1998**, *37*, 4272.
(29) Kinrade, S. D.; Knight, C. T. G.; Pole, D. L.; Syvitski, R. T. *Inorg. Chem.* **1998**, *37*, 4278.

TPA^+. The conductivity at the cac for each solution is directly related to the molar conductivity of the cation with increasing conductivity following the increase in molar conductivity, Λ ($\Lambda_{Cs^+} = 77.26 \times 10^{-4}$ S·m²/mol, $\Lambda_{Na^+} = 50.10 \times 10^{-4}$ S·m²/mol, $\Lambda_{TMA^+} = 44.92$ S·m²/mol, $\Lambda_{TPA^+} = 23.42 \times 10^{-4}$ S·m²/mol).[30] The slopes of both the conductivity and [OH^-] curves for all four cations are nearly the same prior to the cac (~1 OH^-:SiO_2). After the cac, the variation in the slope of the conductivity, however, is proportional to the molar conductivities of the cation, indicating that as the silica concentration increases beyond the cac, a progressively larger fraction of the cations are drawn out of solution into the nanoparticles.

Figure 1A shows also the behavior of solutions at higher and lower initial pHs (29:9500 and 4.5:9500 OH^-/H_2O) for TPAOH solutions. For both curves, a cac is apparent though shifted to a silica ratio equivalent to approximately a 1:1 ratio of $[OH^-]_{initial}/SiO_2$. The same results are observed for Cs^+, Na^+, and TMA^+ at the high and low pH values with cac values varying from 0.176 to 0.196 mol/kg SiO_2 for the 29:9500 OH^-/H_2O solutions and 0.023−0.033 mol/kg SiO_2 for the 4.5:9500 OH^-/H_2O solutions. In a phase diagram of [OH^-] versus [SiO_2], we can then draw a locus of cac's that is independent (within experimental error) of the identity of the cation.

Phase Behavior. Self-assembly typically refers to systems, such as micelles and vesicles, where the process of structure formation is driven by competing forces, such as van der Waals interactions, hydrogen bonding, and electrostatic interactions.[31] The formation of molecular aggregates is thermodynamically an equilibrium process resulting from a decrease in the total chemical potential of the system. When a critical monomer concentration is reached, self-assembly starts leading to a stable suspension of aggregated monomer particles. The silica nanoparticle system displays similar behavior, forming stable nanoparticles at approximately a 1:1 ratio of SiO_2/OH^-. The "monomer" interactions in this system are covalent bonds that would be considered too strong to be within the range of self-assembly. However, the low free energy of formation for these bonds at high pH in an aqueous environment allows the monomer to behave similarly to surfactant molecules. In ref 32, Yang and Navrotsky measured the enthalpies of formation of silicalite-1 crystals in solutions similar to those studied here. The change in enthalpy after the cac is related to the energy released by the formation of Si−O−Si bonds in aqueous solutions (2.5 kJ/mol SiO_2 equal to $kT = 2.49$ kJ/mol at 298 K). In these nanoparticles, the enthalpies of association for SiO_2 are comparable to the enthalpies of association for surfactant molecules.[31] Consequently, although the nature of the interactions is different, the energetics are similar, and thus, it is not surprising that silica can self-assemble.

We have shown that in the presence of TAA^+ cations (TMA^+, TEA^+, TPA^+, TBA^+) silica aggregates into well-defined nanoparticles.[13] Within these systems, silica forms nanoparticles in exactly the same manner as that described in the sodium and cesium systems. The cac's for these solutions are relatively constant with a minimum of 0.049 mol/kg for TBA^+ and a maximum of 0.052 for TMA^+. Since the aggregation process appears independent of the cation used in the solution, the two most important variables affecting the system are OH^- and SiO_2 concentrations. Given that the system behaves as if it were in a local minimum of the chemical potential, it is possible to construct Figure 2 describing in general the phase behavior of the solution for all cations.

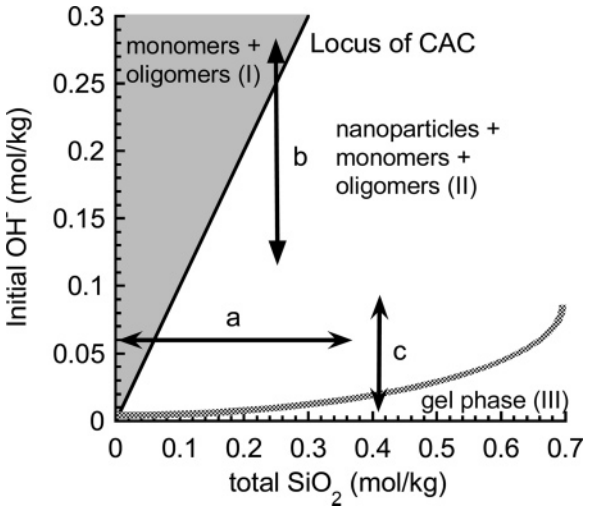

Figure 2. Approximate phase diagram of water soluble silica at high pH. Soluble silica solutions can exist in three different phases in high pH solutions. Region I, in which silica is present as monomers and small oligomers, occurs at molar ratios of SiO_2/OH^- less than 1 (below the cac). Region II exists at molar ratios above 1 and is defined by the formation of nanoparticles which can be measured with small-angle scattering. Region III occurs at higher silica concentrations with a boundary dependent on initial pH and cation type and is defined by the formation of large silica species visible to the eye. For the arrows, see text.

Three distinct regions are present in the phase diagram. The first exists for OH^-/SiO_2 ratios greater than 1. In this region I, SAXS patterns do not show any signal from silica nanoparticles, and an increase in the silica concentration causes a significant decrease in both the conductivity and pH of the solution due to the deprotonation of $Si(OH)_4$. The solution at this stage is composed largely of the deprotonated form of $Si(OH)_4$ with small fractions of oligomeric species and neutral $Si(OH)_4$.[28]

For OH^-/SiO_2 ratios lower than ~1, the SAXS patterns show a signal arising from silica nanoparticles. The onset of nanoparticles coincides with a leveling off of both the conductivity and pH of the solution caused by a change in the dominant reaction.[13] Within this region II, water soluble silica polymerizes, leading to the formation of nanoparticles that reach a size dependent on the pH of the solution. Figure 3A shows the variation in particle size as a function of the initial OH^- concentration at a constant SiO_2/OH^- molar ratio for TPA−silica nanoparticles. The curve follows a logarithmic decrease in the particle size, with R_g decreasing from ~25 Å at low initial OH^- concentration to ~5 Å at an initial molar ratio of 60 TPAOH:9500 H_2O. The pH at the cac follows the opposite trend (Figure 3B), suggesting that the particle size is linked to a charge balance between the solution and the particle. Similar behavior linking nanoparticle size to the solution pH has been reported previously.[14] Our findings here are in contradiction to the general view[7,15,18] of these nanoparticles as having a specific size of 2−5 nm showing that in fact they can be outside this range. Figure 3B also compares the pH at the cac to the predicted pH for amorphous silica.[33] As the silica concentration increases, the equation underpredicts the amount of soluble silica present at a given pH. Since less silica is present in the

(30) Castellan, G. W. *Physical Chemistry*, 3rd ed.; The Benjamin/Cummings Publishing Company, Inc.: New York, 1983.
(31) Israelachvili, J. *Intermolecular & Surface Forces*, 2nd ed.; Academic Press: New York, 1992.
(32) Yang, S. Y.; Navrotsky, A. *Chem. Mater.* **2002**, *14*, 2803.
(33) Alexander, G. B.; Heston, W. M.; Iler, R. K. *J. Phys. Chem.* **1954**, *58*, 453.

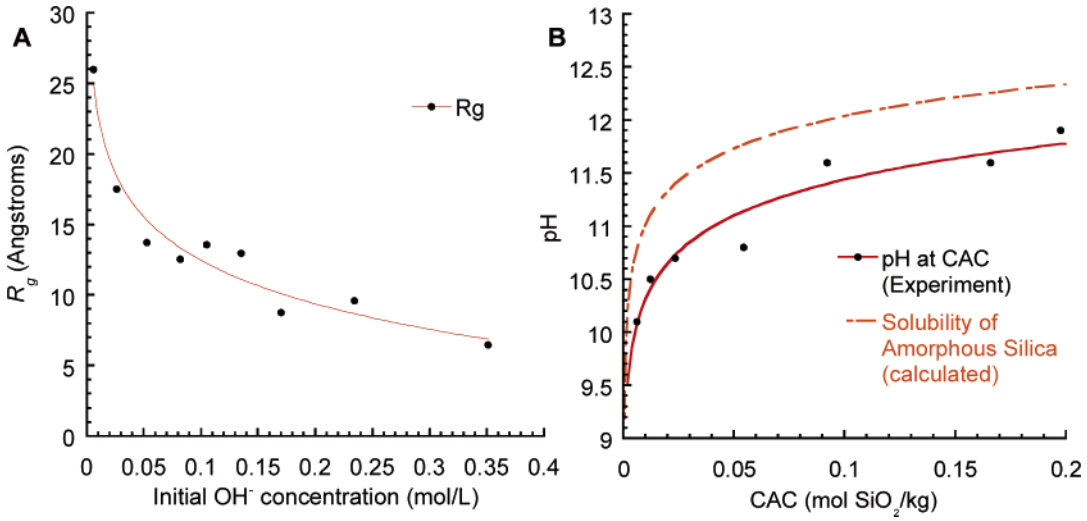

Figure 3. Effect of hydroxide concentration on particle size and silica solubility. (A) R_g as a function of the initial hydroxide concentration of the solution. The particle size shows a logarithmic decrease (red line is a logarithmic fit) as the initial solution pH increases. (B) Solution pH at the cac as of function of the cac. The solid line represents the logarithmic fit of the nanoparticle phase boundary between region I and II. Comparison to a curve (dotted line) fitted to amorphous silica solubility experiments indicates that the nanoparticles are less stable then amorphous silica but display the same trend.

form of nanoparticles than would be predicted for amorphous silica, the nanoparticles are a more stable silica species.

The final region III is characterized by the formation of large silica species. SAXS analyses of this region indicate the presence of nanoparticles; however, in addition to nanoparticles, larger particles, visible to the naked eye, are also present in the solution. At low silica and OH^- concentrations, these particles begin to sediment out of solution; on the other hand, at higher concentrations, these solutions form semisolid gels. The conductivity and pH curves for these systems continue to show the gradual decrease observed in region II, which is caused primarily by the immobilization of the SDA on the nanoparticle surface. The creation of large macroscopic silica species does not cause the removal of either additional SDA or OH^- from the system and may be the result of nanoparticle aggregation. Region III may be a two-phase equilibrium region with solid large silica species and a liquid suspension of nanoparticles similar to those seen in micelle systems.[34] Further description of the properties of the system in region III is beyond the scope of this manuscript.

Reversibility. The equilibrium nature of these solutions was studied first in a series of experiments crossing the cac in several directions. Multiple experiments were conducted to probe the equilibrium along path a and path b (Figure 2). To test the reversibility of path a within region II, we performed a seeded growth experiment consisting of nanoparticles and oligomers as described in Figure 4. A 9 TPAOH:9500 H_2O:40 SiO_2:160 EtOH solution containing nanoparticles was aged for 24 h (C4). Additional silica was added to increase the SiO_2 molar ratio to 60 and aged for another 24 h (C6′). Another solution was prepared with this same final composition (C6). Figure 4 shows the SAXS patterns of these solutions. After 1 day, C6 and C6′ both show a slight increase in size and concentration over C4. However, C6′ has both a higher concentration and a larger particle size than C6. If the same samples, though, are allowed to rest at room temperature for 4 days, the patterns from both C6 and C6′ become indistinguishable. This experiment indicates that the phase behavior of the solution is independent of the path that is taken to prepare

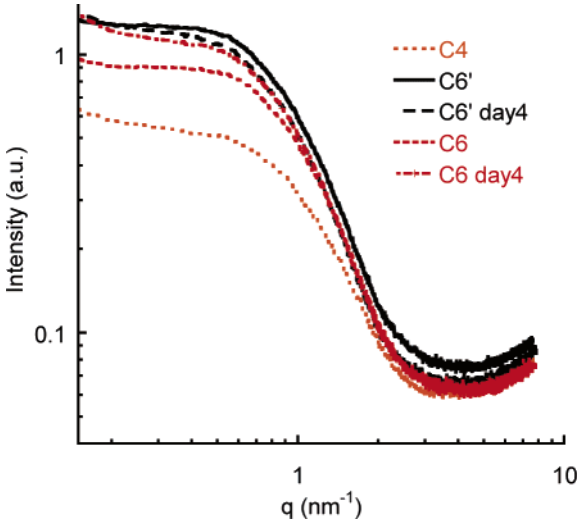

Figure 4. Path independence of particle size and solution structure. Samples with molar ratios of 9 TPAOH:9500 H_2O:60 SiO_2:240 EtOH are prepared by two different methods: complete addition of silica on day 1 (C6) and stepwise addition over 2 days (C4 to C6′). SAXS patterns display differences in particle size and concentration between C6 (- - -), C6′ (—), and C4(• • •) after 1 day. C6 and C6′ are indistinguishable by day 4.

it, as expected for an equilibrium process. Similar measurements along path a ranging from SiO_2 molar ratios of 40 to 80 display similar particle sizes (nanoparticle volume variations of approximately 15%) with a linear increase in the particle concentration. Diluting these solutions into region I causes dissolution of the nanoparticles.

Path b involves the increase and decrease of solution pH through the addition of TPAOH or HBr. Decreasing the solution pH below the cac causes the formation of nanoparticles. Similar nuclear magnetic resonance (NMR) measurements performed by Kinrade et al.[28] for TMAOH showed that decreasing the pH below the cac caused sharp peaks characteristic of small silica species to broaden into peaks characteristic of nanoparticles. As the OH^- concentration is increased into region I, particles dissolve completely except in cases of high pH with silica concentrations close to the cac. In these cases, particles may

(34) Clint, J. H. *Surfactant Aggregation*; Chapman and Hall: New York, 1992.

exist at silica concentrations within region I, but the size of these particles is significantly reduced.[13]

There are two explanations for the observation of scattering intensity prior to the cac at high silica concentrations: either a broadening of the local minimum of the chemical potential or the concentration of oligomeric species is high enough to be detected. In self-associating systems with a definite critical point of aggregation, the chemical potential of the particle exhibits a deep minimum with respect to size.[31] A broadening of the minimum of the chemical potential may be caused by variations in attractive and repulsive forces governing particle formation (which are strongly affected by pH), leading to cac broadening. At low pH, the system appears to have a steep minimum in the chemical potential and exhibits a sharp cac, but at higher pH, the cac is no longer a sharp point (as determined by SAXS); that is, nanoparticles can form prior to the predicted cac. For example, studying solutions with molar compositions of 9 TPAOH:480 H_2O, Yang and Navrotsky[3] found that during gradual TEOS addition the hydroxide concentration followed the same behavior reported here. They reported the formation of small nanoparticles (~5 Å) prior to the cac which may fall into the broad cac region. We have found that the scattering patterns of solutions prepared with TMAOH, TEAOH, and TPAOH at the reported concentration (9 M^+OH^-:480 H_2O:8 SiO_2:32 EtOH) are all similar. Note that the size of these nanoparticles is of the same order as cubes of silica formed in the presence of TMA.[28] These oligomeric species could also be present in the lower pH solutions prior to the cac but in concentrations below our detection limit.

Unlike the cac for these systems, the cation type plays a significant role in the position of the phase boundary between regions II and III. With increasing TEOS concentration, large particles first appear in solutions of NaOH followed by CsOH and then TPAOH. The boundary point can be studied qualitatively by measuring the system R_g, which increases rapidly as the boundary is crossed. Specifically, R_g of the nanoparticles for systems with the same initial pH increased from 8.8 to 14 Å for TPAOH, 11.8 to 29.6 Å for CsOH, and 10 to greater than 35 Å for NaOH with increases in the SiO_2/OH^- molar ratio from 2 to 5. A study of the boundary between regions II and III will be the subject of a future report.

Structure of TPA−Silica Nanoparticles. In this section, we determine the structure of TPA−silica nanoparticles quantitatively. Figure 5 compares an analytical sphere PDDF to the experimental SANS PDDF of the TPA−silica nanoparticle (9 TPAOH:9500 H_2O:40 SiO_2:160 EtOH). The experimental PDDF is broader, and this difference could be rationalized by two possibilities; namely, either the particle has an elongated shape similar to a cylinder or an ellipse or the particles are polydisperse (or both). Below, we examine both possibilities.

Analysis of SANS/SAXS data to yield a specific particle morphology requires that all plausible structural models are tested. To do so, relevant parameters, such as the particle SLD and density, are first determined for use in model fitting. Next, simple uniform particle models are used to narrow the range of possible particle shapes by fitting the form factor of the SANS pattern. Core−shell and polydisperse models are tested by fitting the form factor to both SAXS and SANS patterns followed by the inclusion of the structure factor to reach the optimal solution while accounting for the effects of interparticle interactions. The data presented here is for nanoparticles prepared with TPAOH (9 TPAOH:9500 H_2O:40 SiO_2:160 EtOH), at room temperature for which we measured

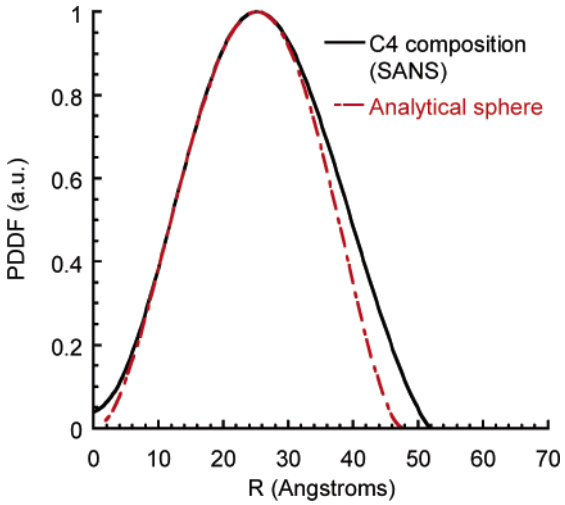

Figure 5. Comparison of TPA nanoparticle SANS PDDF with an analytical sphere. The curves deviate following the peak maximum. The increased width of the distribution obtained from SANS can be attributed to elongated particles or polydispersity.

scattering patterns for both SAXS and SANS with good signal-to-noise levels.

Contrast matching experiments lead to particle scattering lengths of 2.22×10^{-6} and 5.95×10^{-6} Å^{-2} for solutions prepared with h_{28}-TPAOH and d_{28}-TPAOD, respectively. These values are used in all SANS data analysis of particle shapes with uniform composition. To simulate particles with core−shell structures, the SLD of the core (silica + H_2O) is estimated as 2.32×10^{-6} Å^{-2} on the basis of a density of 1.75 g/cm^3. This density was determined from density gradient experiments conducted on the silica material isolated from the final synthesis solution following the isolation procedure of ref 5. (The density values are scattered between 1.7 and 1.8 g/cm^3.) Variations in the density between 1.6 and 1.8 g/cm^3 result in a less than 5% variation in the final particle volume (see below). The shell SLD is estimated as 0.46×10^{-6} Å^{-2} from crystalline h_{28}-TPAOD with lattice parameters based on the structure of crystalline TPABr.[35] Note that we do not have direct evidence indicating that there is no TPA^+ in the core. However, the independence of core size and shape upon changes in the cation size is a good indication that the core is mostly cation free.

Table 1 lists the optimized values for the particle dimensions, the volume fraction, the solution background, and the "goodness" of fit, χ (a smaller χ indicates a better fit). For various particle shape models, Figure 6 shows the results of fitting the measurements to uniform spheres, cylinders, and polydisperse spheres with corrections for instrumental smearing. Sphere and polydisperse sphere forms fail to fit the pattern at high q values as seen from the deviation between experimental data and simulations at approximately $q = 0.15$ Å^{-1}. Cylinders and oblate ellipsoids can fit the change in slope and represent the best uniform particle fits.

Even though uniform particles of cylinder and oblate ellipsoidal shapes are capable of capturing the major features of the patterns, the agreement between measurement and simulation is greatly improved when core−shell models are used. From our previous comparison of the R_g values of SAXS and SANS patterns (14.9 Å for SAXS and 26.8 Å for SANS), it is clear that the particles have a core−shell type of structure.[13] In the simulation,

(35) Zalkan, A. *Acta Crystallogr.* **1957**, *10*, 557.

Table 1. Results from Simulations of SANS Patterns for Nanoparticles Formed at 9 TPAOH:9500 H_2O:40 SiO_2:160 EtOH and 9 TMAOH:9500 H_2O:40 SiO_2:160 EtOH (Annotation: e^- Represents Total Nanoparticle Charge)

TPA^+ Nanoparticles

shape	dimensions (Å)	SLD × 10^6 (Å^{-2})	χ^2	other parameters
		Uniform Particles		
sphere	R = 31.8	2.17	9434	
cylinder	R = 36.1 H = 27.4	2.17	1255	
polydisperse sphere	R(av) = 21.7	2.17	4293	polydispersity = 0.42
prolate ellipse	R(major) = 52.7 R(minor) = 24.6	2.17	2908	
oblate ellipse	R(major) = 41.3 R(minor) = 16.0	2.17	1293	
		Core−Shell Particles		
oblate ellipse	R_{core}(major) = 30.2 R_{core}(minor) = 8.3 R_{shell}(major) = 39.0 R_{shell}(minor) = 14.2	shell = −0.41 core = 3.47 solvent = 6.39	1247	
cylinder	R_{core} = 28.6 R_{shell} = 5.9 H = 12.6	shell = −0.41 core = 3.47 solvent = 6.39	1308	
polydisperse sphere	R(av) = 13.9 shell thickness = 8.7	shell = −0.41 core = 3.47 solvent = 6.39	1992	polydispersity = 0.44
		Structure Factor		
core−shell oblate ellipse	R_{core}(major) = 33.8 R_{core}(minor) = 6.8 R_{shell}(major) = 39.9 R_{shell}(minor) = 13.6	shell = −0.41 core = 3.47 solvent = 6.39	473	charge = 191 e^- solvent dielectric = 70.74 monovalent salt = 0.052 M temperature = 298 K

TMA^+ Nanoparticles

shape	dimensions (Å)	SLD·10^6 (Å^{-2})	χ^2	other parameters
core−shell oblate ellipse	R_{core}(major) = 30.0 R_{core}(minor) = 4.0 R_{shell}(major) = 31.0 R_{shell}(minor) = 7.0	shell = −0.51 core = 3.47 solvent = 6.39	355	charge = 106 e^- solvent dielectric = 70.74 monovalent salt = 0.052 M temperature = 298 K

the SLD of TPAOD is allowed to vary, whereas the SLD of silica in the core and the solvent are held constant. The oblate ellipse yields the best overall fit with major radii of 29 and 37 Å for the core and core−shell, respectively, and minor radii of 8 and 14 Å, respectively. These values are comparable to the dimensions of the silica core ellipsoid determined from SAXS measurements (major radius, 21 Å; minor radius, 10 Å) with approximately one monolayer of TPA^+ on the surface. These measurements are independent of the ratio of D_2O/H_2O in the synthesis with

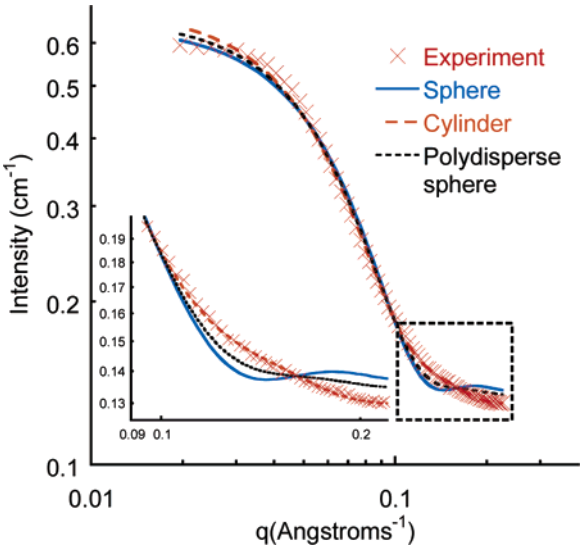

Figure 6. Fitting of SANS pattern for TPA nanoparticles assuming uniform composition. All particle shapes display similar deviations in the low q region from 0.2 to 0.6 Å^{-1}. At higher q values above 0.1 Å^{-1} (see inset), only elongated shapes can capture the change in curvature.

SAXS patterns for nanoparticles prepared in D_2O having the same pattern as those prepared in H_2O. The smaller size of the major radii of the core (21 Å for SAXS vs 29 Å for SANS) may result from the fact that the particle surface is composed of a significant number of silanol units which have SLD values similar to the solvent leading to an effective smaller core size using SAXS than with SANS. In addition, a monolayer of water may exist between the silica core and the organic shell. Schematic representations for the ellipsoidal and cylindrical particles, which represent the best form factor fits, are shown in Figure 7. On the basis of our density range of 1.6−1.8 g/cm^3 and particle volume, the core size of the ellipsoidal particle consists of 250−300 SiO_2 units.

It is possible that a polydisperse set of core−shell spherical particles could also fit the scattering curves at high q as well as the ellipsoidal model. Applying the polydisperse core−shell model (NIST)[26] to our SANS measurements yields polydispersity values of approximately 0.4 and core radii of 16 Å on the basis of a

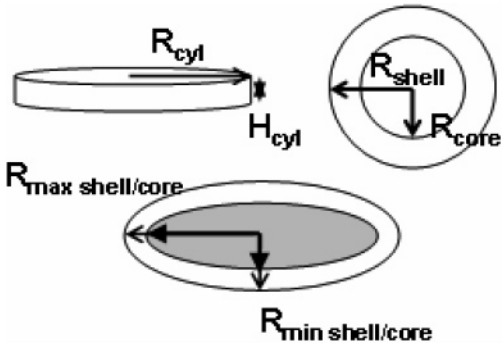

Figure 7. Diagram of particle structures used in least-squares fitting of SANS data.

rectangular distribution for the polydispersity. We apply the same definition for the polydispersity, which is the standard deviation of the distribution divided by the average particle radius, as the NIST fitting software.[26] In fact, both the core−shell cylinder and ellipse are better fits than the polydisperse core model, although the polydisperse core−shell model is an improvement over the sphere models.

To exclude the possibility of significant nanoparticle polydispersity, a simultaneous analysis of SAXS and SANS patterns was used. We use the polydispersity of the particle's core as the key factor to establish if the polydisperse model is physically feasible, since the particle's shell should remain of constant radius if only a monolayer of TPA^+ adsorbs onto the surface of the particles.[36,37] The core polydispersity determined for both the SANS and SAXS patterns should be nearly the same. For the SAXS pattern, the PDDF of a Gaussian distribution of spherical objects can be determined by summing over the individual PDDF curves of analytical spheres[24] multiplied by the fraction of particles predicted to have a given radius from the Gaussian distribution. The maximum of the experimental PDDF is used as the center of the Gaussian distribution with the standard deviation optimized to yield the best fit to the experimental data. The best fit to the SAXS data gives a mean particle size of 18.3 Å and a standard deviation of 3.6 Å, which yields a polydispersity of 0.20 significantly different from that predicted from the simulation of the SANS patterns. We have tested further the effect of polydispersity following procedures developed for microemulsions[21,22] and found that applying a Gaussian distribution of core sizes to the SANS pattern yielded approximately the same final solution as the fitting procedure with an average core radii of 16 Å and a polydispersity of 0.4. We thus conclude that the overall best fit to the SAXS and SANS patterns is the monodisperse oblate ellipsoid, though more rigorous modeling may validate a polydisperse or cylindrical solution that is consistent with the experimental data.

Figure 8 displays the final fitted SANS pattern including the minor effects of the Hayter−Penfold approximation for the structure factor. The Hayter−Penfold approximation assumes a sample of uniform spherical particles that have a net charge, e^- (electrons). It is possible to use this structure factor for nonspherical particles using the decoupling approximation, as recently shown by Bergstrom for tablet shaped particles.[38] The scattering cross section, $d\sigma(q)/d\Omega$, in the decoupled case is defined as

$$\frac{d\sigma(q)}{d\Omega} = (\rho_{particle} - \rho_{solvent})^2 M\langle F^2(q)\rangle_0 \times \left(1 + \frac{\langle F(q)\rangle_0^2}{\langle F^2(q)\rangle_0}(S(q) - 1)\right) \quad (5)$$

where M is the molecular mass of the nanoparticle. The structure factor for the nanoparticles was analyzed using eq 5 with an oblate ellipse model for the form factor with varying aspect ratios ranging from spheres to very thin platelike particles. The inclusion of particle shape (last term in eq 5) only led to small deviations in the simulated structure factor when compared to the basic Hayter−Penfold model. Consequently, we have used the Hayter−Penfold structure factor for spherical particles with an effective diameter based on the form factor parameters to include interparticle force effects in the simulation of the scattering patterns.[26]

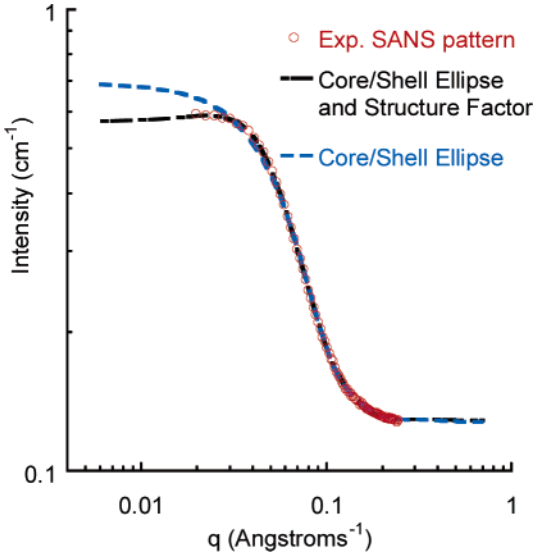

Figure 8. Experimental and fitted SANS patterns of TPA nanoparticles using core−shell models. A structure factor including the effects of electrostatic forces between TPA nanoparticles is added to the best fit particle shape solution (the oblate core−shell ellipsoid) capturing the low q characteristics of the SANS pattern.

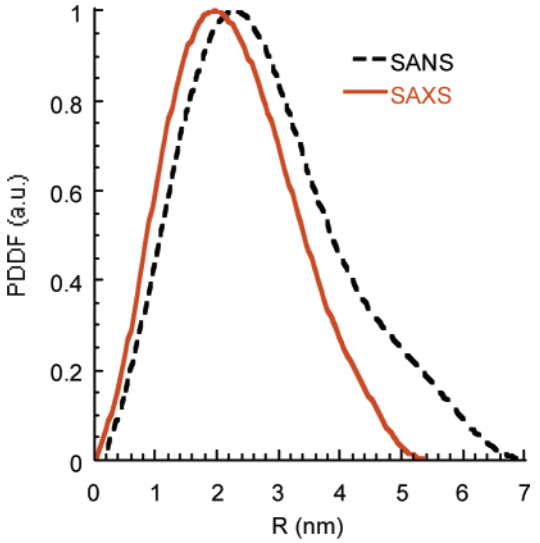

Figure 9. Neutron and X-ray PDDFs for TMA nanoparticles. The TMA nanoparticle displays the same core−shell structure observed for the TPA nanoparticle.

We performed the same structural analysis for nanoparticles formed with TMAOH and found similar final results. As with the TPAOH nanoparticle, SAXS and SANS measurements can be described well by a core−shell particle structure (Figure 9). Complete analysis of the SANS scattering patterns yielded an oblate ellipse as the best fit for the nanoparticle core with a major radius of 30 Å and in line with a SAXS fit of 28 Å. The optimal shell thickness is a thinner layer than that possible for a layer of TMA^+. This difference may be due to multiple factors including surface roughness and particle density gradients, both of which will require more detailed models.

(36) Tetraalkylammonium cations have been shown to form aggregates in water solutions but only at molarities (1 mol/L)[29] well above those in our studies (0.052−0.35 mol/L), so we do not expect multilayers or TAA^+ aggregates in the system to affect polydispersity.

(37) Wen, W.; Saito, S. *J. Phys. Chem.* **1964**, *68*, 2639.
(38) Bergstrom, M.; Pedersen, J. S. *J. Phys. Chem. B.* **1999**, *103*, 8502.

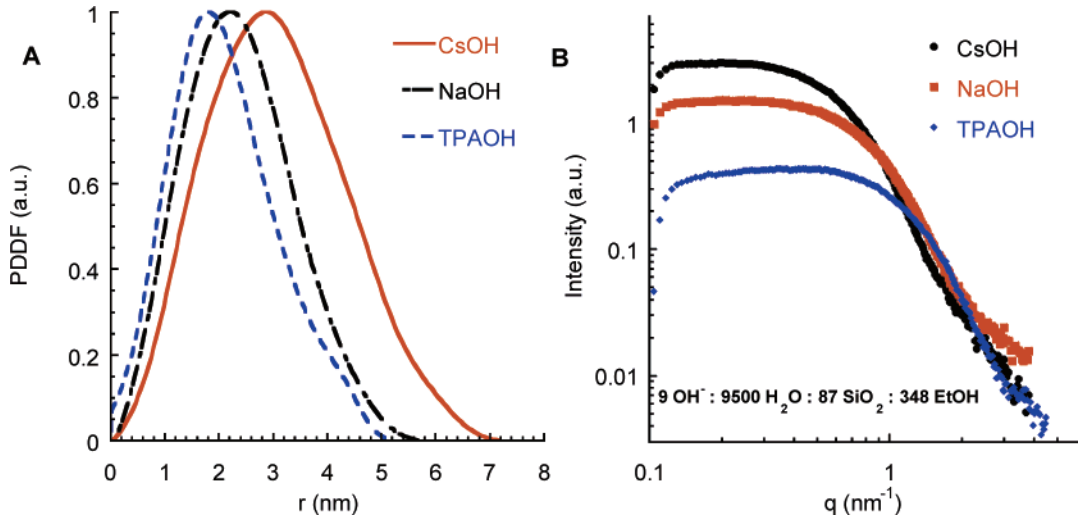

Figure 10. Particle morphology of inorganic cation nanoparticles. (A) PDDFs of the SAXS patterns. Cs and Na particles appear to have a larger particle size than TPA in SAXS patterns. The PDDF shape indicates the particles are not spherical. (B) SAXS pattern of nanoparticles of Cs^+, Na^+, and TPA^+. The PDDFs indicate variations in the nanoparticle size between the three cations as well as concentration differences.

The PDDF of the SAXS and SANS patterns demonstrate conclusively that there is a TMA^+ layer surrounding the particle.

Microstructure of the Nanoparticles in the Presence of Inorganic Cations. We have shown through the comparison of SAXS and SANS patterns that silica–TPA nanoparticles have a core–shell structure with silica in the core and TPA^+ mostly in the shell. Analysis of TMA^+ solutions displays this same core–shell particle structure. However, it remains to be determined whether these observations can be extended to inorganic cations.

The SAXS patterns for Na^+, Cs^+, and TPA^+ solutions (Figure 10A) show a distinct peak at nearly the same q value, while an IFT[27] analysis of the PDDFs calculated from these SAXS patterns (Figure 10B) with compositions of 9 R^+OH^-:9500 H_2O:40 SiO_2:160 EtOH indicates that all particles are similar (elongated shapes) but with slightly different sizes. We attempted to verify the size of the particles with SANS for the Na^+OD^- system; the analysis of the scattering data indicates that the particles have an ellipsoidal shape with dimensions similar to that obtained from the SAXS patterns. Further analysis was not possible due to the relatively weak scattering signal. Note that, unlike TPA^+ and TMA^+, the X-ray scattering contrast between the Na^+ and Cs^+ ions and water is a factor of 10 higher (1.1×10^{-7} Å^{-2} for TPA^+ and -1.51×10^{-6} Å^{-2} for Na^+). Even with the inclusion of a hydration sphere of water surrounding the Na^+ ion, the contrast is 5 times greater, allowing for the nanoparticle shell to be observed in SAXS. Consequently, inorganic cations should be easily observed in the SAXS patterns. For instance, the R_g calculated from these PDDFs increases from 15 Å for TPA^+ to 23.5 Å for Cs^+ (see Table 2). A comparison of the SAXS PDDF in Figure 10B with the SANS PDDF of TPAOH (Figure 11) is revealing. Both the TPAOH and CsOH PDDFs have the same maximum value. The only difference between the two is a slight increase in nanoparticle size in the TPAOH case which can be attributed to the large cation size. The similarity of these two PDDF patterns and macroscopic behavior of the solutions strongly indicate that the Cs and TPA particles have the same core–shell structure.

Summary and Conclusions

The formation of silica nanoparticles at room temperature has been studied in both inorganic and organic strong base solutions. For all strong base solutions studied here and in our previous report,[13] a critical point for nanoparticle formation (cac) has been shown to exist at ~1:1 SiO_2/OH^- ratio. Prior to this critical point, no nanoparticles are detected in solution, and the addition of small amounts

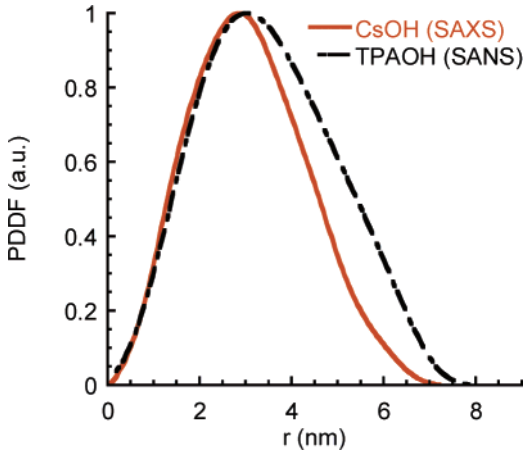

Figure 11. Comparison of Cs nanoparticle X-ray PDDF with TPA nanoparticle neutron PDDF. The apparent increase in particle size displayed in the SAXS pattern is caused by the increase in cation scattering cross section. For Cs, the surface cation layer is observed in the SAXS pattern leading to a similar PDDF distribution as a SANS pattern of a TPA nanoparticle where the surface cation layer is also visible. The larger size for the TPA nanoparticle is related to the difference in size between the two cations.

Table 2. Summary of Critical Aggregation Concentrations and Nanoparticle Radii of Gyration

Initial composition	cac from [OH^-] (mol of SiO_2/kg)	cac from conductivity (mol SiO_2/kg)	R_g (Å)
9 TMAOH:9500 H_2O	0.058	0.052	17.7
9 TPAOH:9500 H_2O	0.056	0.054	14.9
9 NaOH:9500 H_2O	0.055	0.047	18.3
9 CsOH:9500 H_2O	0.058	0.055	23.5
29 TPAOH:9500 H_2O	0.176	0.185	8.8
4.5 TPAOH:9500 H_2O	0.024	0.024	20.1
4.5 TMAOH:9500 H_2O	0.028	0.034	20.4
4.5 NaOH:9500 H_2O	0.026	0.027	19.5
4.5 CsOH:9500 H_2O	0.022	0.029	20.4
29 TMAOH:9500 H_2O	0.181	0.184	8.7
29 NaOH:9500 H_2O	0.181	0.182	32.5
29 CsOH:9500 H_2O	0.17	0.196	29.6

of silica monomer in the form of TEOS only results in the deprotonation of $Si(OH)_4$, as was previously known.[12] After the cac, silica condensation leads to charged nanoparticles with an oblate ellipsoidal shape as the best fit of our data. These particles show a pseudoequilibrium phase behavior with three distinct regions: a monomer/oligomer region prior to the cac, a monomer/oligomer/nanoparticle region after the cac, and a gel region at high SiO_2/OH^- ratios. Nanoparticle formation is reversible through suitable addition or removal of SiO_2 or OH^-. Within the nanoparticle region, the particle size appears to be closely linked to the initial concentration of OH^- in solution.

Acknowledgment. This work was funded by the National Science Foundation under Grant No. 0103010. We acknowledge Stephen Ekatan for his assistance with the TMAOH experiments and David Kragten and Jeff Rimer for their assistance in gathering the SANS data. The X-ray experiments were made with a SAXSess small-angle X-ray instrument on loan from Anton Paar GmbH, in Graz/Austria. This work utilized facilities supported in part by the National Science Foundation under Agreement No. DMR-9986442. We acknowledge the support of the National Institute of Standards and Technology, U.S. Department of Commerce, in providing the neutron research facilities used in this work.

LA0468390